The archaeal LDH-like malate dehydrogenase from Ignicoccus islandicus displays dual substrate recognition, hidden allostery and a non-canonical tetrameric oligomeric organization

Jennifer Roche, Eric Girard, Caroline Mas, Dominique Madern

▶ **To cite this version:**

Jennifer Roche, Eric Girard, Caroline Mas, Dominique Madern. The archaeal LDH-like malate dehydrogenase from Ignicoccus islandicus displays dual substrate recognition, hidden allostery and a non-canonical tetrameric oligomeric organization. Journal of Structural Biology, 2019, 10.1016/j.jsb.2019.07.006 . hal-02273509

HAL Id: hal-02273509
https://hal.science/hal-02273509

Submitted on 20 Jul 2022

HAL is a multi-disciplinary open access archive for the deposit and dissemination of scientific research documents, whether they are published or not. The documents may come from teaching and research institutions in France or abroad, or from public or private research centers.

L'archive ouverte pluridisciplinaire **HAL**, est destinée au dépôt et à la diffusion de documents scientifiques de niveau recherche, publiés ou non, émanant des établissements d'enseignement et de recherche français ou étrangers, des laboratoires publics ou privés.

Distributed under a Creative Commons Attribution - NonCommercial 4.0 International License

Version of Record: https://www.sciencedirect.com/science/article/pii/S1047847719301534
Manuscript_1e28afb1ed0f5446afee55dd2fecad2d

The archaeal LDH-like malate dehydrogenase from *Ignicoccus islandicus* displays dual substrate recognition, hidden allostery and a non-canonical tetrameric oligomeric organization.

Jennifer Roche, Eric Girard, Caroline Mas and Dominique Madern*

Univ. Grenoble Alpes, CEA, CNRS, IBS, 38000 Grenoble, France

* Corresponding author:

Dr Dominique Madern, Institut de Biologie Structurale, Campus EPN CS 10090, 71 avenue des Martyrs, 38044 Grenoble Cedex 9; France.

Email: dominique.madern @ ibs.fr. Phone: 33- (0) 4 57 42 85 71.

© 2019 published by Elsevier. This manuscript is made available under the CC BY NC user license
https://creativecommons.org/licenses/by-nc/4.0/

Abstract

The NAD(P)-dependent malate dehydrogenases (MalDHs) and NAD-dependent lactate dehydrogenases (LDHs) are homologous enzymes involved in central metabolism. They display a common protein fold and the same catalytic mechanism, yet have a stringent capacity to discriminate between their respective substrates.

The MalDH/LDH superfamily is divided into several phylogenetically related groups. It has been shown that the canonical LDHs and LDH-like group of MalDHs are primarily tetrameric enzymes that diverged from a common ancestor. In order to gain understanding of the evolutionary history of the LDHs and MalDHs, the biochemical properties and crystallographic structure of the LDH-like MalDH from the hyperthermophilic archaeon *Ignicoccus islandicus* (*I. isl*) were determined. *I. isl* MalDH recognizes oxaloacetate as main substrate, but it is also able to use pyruvate. Surprisingly, with pyruvate, the enzymatic activity profile looks like that of allosteric LDHs, suggesting a hidden allosteric capacity in a MalDH. The *I. isl* MalDH tetrameric structure in the apo state is considerably different from those of canonical LDH-like MalDHs and LDHs, representing an alternative oligomeric organization. A comparison with MalDH and LDH counterparts provides strong evidence that the divergence between allosteric and non-allosteric members of the superfamily involves homologs with intermediate, atypical properties.

Keywords. Allostery; lactate and malate dehydrogenase; archaea; molecular evolution; quaternary structure; crystallophore.

1. Introduction

Lactate dehydrogenases (LDHs) (EC 1.1.1.27) and Malate dehydrogenases (MalDHs) (EC 1.1.1.37) belong to a wide group of 2-ketoacid:NAD(P)-dependent dehydrogenases that catalyze the reversible conversion of 2-hydroxyacids to the corresponding 2-ketoacids (Holbrook et al., 1975). Both enzymes are involved in energy metabolism. LDHs operate at the final stage of aerobic glycolysis and MalDHs are involved in the citric acid cycle. They share the same protein fold and a similar catalytic mechanism (Birktoft & Banaszak, 1983; Clarke et al., 1986; Hart et al., 1987 a, b; Clarke et al., 1988; Waldman et al., 1988). When the competent catalytic state is reached, LDH catalyzes the direct transfer of a hydride ion from the pro-R face of NADH to the C2 carbon of pyruvate to produce lactate, whereas MalDH transforms oxaloacetate into malate (Burgner and Ray, 1984; Ferst, 1985).

Crystallographic structures of both enzymes have allowed the detailed description of NADH and substrate binding sites (Iwata et al., 1994, González et al., 2018). Pyruvate and oxaloacetate are keto acids that share a common carboxylate extremity, which is recognized within the catalytic site by the positively charged lateral chain of Arg171, a universally conserved substrate binding residue in LDHs and MalDHs (Birkoft et al., 1982).Residue numbering is done according to the one used for LDH (Eventoff et al., 1977). Upon formation of the transition state, the active-site loop covers the catalytic site allowing its dehydration and the correct anchoring of the substrate by additional interactions due to the nature of the amino acid at position 102 (Iwata et al., 1994). Canonical LDH structures revealed that the polar lateral chain of Gln102, located on the mobile active-site loop, compresses the methyl of pyruvate and contributes to its correct orientation in the catalytic site (Iwata et al., 1994). While in MalDHs, the lateral chain of Arg102 contributes to the screening of the second carboxylate extremities of oxaloacetate (Birkoft et al., 1982). The amino acid at position 102 is therefore considered as the most important substrate-discriminating residue between LDHs and MalDHs. Mutagenesis experiments have demonstrated that the mutation Gln102 to Arg on the catalytic loop converts a LDH into a MalDH (Wilks et al., 1988). The functional conversion from MalDH to LDH by the replacement of Arg102 to Gln, however, has been much less successful

(Cendrin et al., 1993; Boernke et al., 1995). The exact reason for this lack of complete functional reversibility between these enzymes is still not fully resolved. It could be due to long range epistatic effects, i.e interactions between amino acids that enhance or decrease the consequence of a mutation depending on the presence or absence of other amino acids (Harms & Thornton 2010).

Even if the LDH/MalDH superfamily is split into two main functional groups, phylogenetic studies have revealed profound differences within MalDHs, dividing these into two sub-groups with specific properties (Madern, 2002; Madern et al., 2004, Boucher et al., 2014). Most of the bacterial LDHs are tetrameric enzymes that exhibit sigmoidal pyruvate saturation curves in the absence of fructose 1, 6-bisphosphate (FBP), indicating substrate homotropic activation on the enzyme reaction. In the presence of FBP, the enzymatic activity profile of allosteric LDHs becomes hyperbolic demonstrating heterotropic allosteric activation (Arai et al., 2011). In contrast, eukaryotic LDHs are considered to be non-allosteric, even if a protein dynamics study suggested movements reminiscent of allosteric properties (Katava et al., 2017). In the first MalDH sub-group, made up of mitochondrial and cytosolic clades (Madern, 2002; Madern et al., 2004, Boucher et al., 2014, all enzymes are dimeric. In the second sub-group, primary sequences of MalDH display stronger identity with LDHs than with the mitochondrial and cytosolic clades of MalDHs. They have been identified as LDH-like MalDHs, and most of them are tetrameric (Madern, 2002). LDH-like MalDHs are identified under accession numbering (01339) in the Conserved Domain Database (CDD) (Marchler-Bauer et al., 2011). LDH-like MalDHs are mainly found in Bacteria and Archaea, with an exception within the Alveolate (Madern, 2002; Madern et al., 2004, Boucher et al., 2014).

The folding and association pathway has been analyzed for the LDHs and LDH-like MalDHs; it involves a series of sequential steps. In the first, monomers in a molten globule state become more compact upon the formation of active dimeric species and in the second step the dimeric species condense to form active tetramers (Madern et al., 2000 and references therein). Abundant structural information has been obtained from the crystal structures of LDHs and LDH-like MalDHs (Dalhus et al., 2002; Irimia et al., 2003; Coquelle et

al., 2007). The tetramer subunits are related by three molecular 2-fold axes named P, Q, and R (Rossmann et al., 1973).The tetramers of LDHs have four active sites and two FBP-binding sites. These latter sites, which are involved in heterotropic allostery, are absent in LDH-like MalDHs, so that these enzymes are considered as non-allosteric. In LDHs and LDH-like MalDHs, the active site of each subunit lies near the interface along the Q-axis.

Since it was established that LDHs and LDH-like MalDHs diverged from a common ancestral gene (Madern, 2002), numerous Archaeal genome sequences of species from the *Crenarchaeota* phylum were deposited in Data Bank. In this phylum, several species from the *Thermoprotei* class display a single gene sequence encoding putative MalDHs with stronger LDH sequence similarity compared to other LDH-like MalDHs, as it can be identified by Blast searches against Protein Data Bases. Consequently, MalDHs from the *Thermoprotei* class provide an appropriate reservoir of new MalDH/LDH homologs for investigating fundamentals of molecular evolution mechanisms within the whole super family.

In the present work, biochemical and structural properties of the putative MalDH from *Ignicoccus islandicus* (*I. isl* MalDH) were determined, in order to shed light on the peculiar relationship between LDHs and MalDHs from *Crenarchaeota*. The enzymatic characterization showed that the encoded protein is a MalDH, which preferentially uses oxaloacetate as substrate. However, it has a relaxed capacity of substrate recognition allowing it to use pyruvate as substrate, by virtue of an unexpected homotropic activation mode. The *I. isl* MalDH crystal structure was solved; it shows a new quaternary geometry between active dimers within the tetramer. The peculiar configuration was confirmed by solution SAXS measurements. The structure was, furthermore, compared to homologous enzymes of the superfamily to yield insights into the structural bases of the quaternary assembly and activity differences.

2. Results and discussion

In order to facilitate comparison between primary sequences of enzymes analyzed in this work and their structural representation, residue numbering was normalized with respect to the

nomenclature system proposed for Lactate dehydrogenases (Eventoff et al., 1977). With this numbering, important active site residues are labeled Gln102, Arg109, Asp168, Arg171, and His195. In the linear numbering of *I. isl* MalDH, equivalent positions are 86, 92, 151, 154 and 178.

2.1. Quaternary assembly of I. isl MalDH in solution

I. isl MalDH elutes as a single peak on SEC. The experimental weight-averaged molecular mass measured by combining online MALLS and differential refractive index measurements, was 124 ± 6 kDa, in agreement with the theoretical molecular weight of 133 for a tetrameric association (**Fig.1**).

2.2. Enzymatic properties of I. isl MalDH

The primary investigations were aimed to determine the co-enzyme preference of *I. isl* MalDH. Various salt concentrations and pH conditions were tested and, in all the cases, no significant oxaloacetate (OAA) reduction was detected when NADPH was used as coenzyme at 70°C. Consequently, our investigations were performed using NADH. In most of the MalDHs studies, $K_{m\ NADH}$ values were found in the range 0.05-0.15 mM (Lee et al., 2019). To ensure a non-limiting concentration, the enzymatic activity measurements using *I. isl* MalDH were done with a concentration of 0.4 mM NADH. As it is well documented with LDHs (Tomita et al., 2006 and references therein), the presence of an aspartic residue at position 54 of the alignment (**Fig. S1)** suggested *I. isl* MalDH would use NADH instead of NADPH. The lack of NADPH recognition confirmed it is the case. In LDHs, Asp54 is universally conserved and no NADPH-dependent enzyme has been reported to date. Amongst archaeal LDH-like MalDHs from *euryarchaeota* clear cut coenzyme preferences are well established. Most of these euryarchaeal enzymes, which display an Asp at position 54, only use NADH (Cendrin et al., 1993, Langelandsvik et al., 1997). In contrast, those characterized as NADPH-dependent MalDHs have a glycine residue at this position. This is because the

smaller size of glycine allows accommodating the additional phosphate of NADPH (Madern, 2000). Other studies using MalDHs from *crenarchaeota* reported dual coenzyme recognition even if they have an aspartic residue at position 54, suggesting other residues modulate coenzyme specificity (Hartl et al., 1987; Lee et al., 2019)

The *I. isl* MalDH saturation curves for OAA (**Fig. 2**), shows an inhibition by high concentration of substrate. To the best of our knowledge, MalDHs display a stringent capacity of substrate recognition preventing the use of pyruvate as substrate, because they cannot tolerate charge imbalance within their catalytic site (Wilks et al., 1988, Chapman et al., 1999). Surprisingly, it was found that *I. isl* MalDH not only used pyruvate as substrate but also exhibited a sigmoidal-shaped recognition profile (**Fig. 2**), which resembles the one encountered during homotropic activation of allosteric LDHs. The catalytic efficiency (as expressed by k_{cat}/K_m) with OAA (table 1) does not significantly differ from that generally observed with MalDHs. When pyruvate is used instead of OAA, the efficiency drops (table 1). The log value (= 3. 4) of the ratio between (k_{cat}/K_m) for each substrate indicates *I. isl* MalDH strongly prefers OAA by three orders of magnitude compared to pyruvate. Such a result was expected due to the presence of an arginine at position 102 of the sequence alignment (**Fig. S1**). Because of the strong sequence similarity with LDHs, the putative activation of *I. isl* MalDH activity by the allosteric effector of LDH (fructose 1, 6 bis phosphate (FBP)) was tested, with both OAA and pyruvate as substrates. No FBP activation was recorded whatever the condition tested.

Even if the catalytic efficiency of *I. isl* MalDH with pyruvate is weak, the unexpected sigmoidal profile with this substrate is an interesting issue. It suggests that *I. isl* MalDH behavior resembles that of allosteric LDHs. Allosteric transition of LDHs fits well the recent model of allostery (Motlag et al., 2014 and references therein), as well as the Monod-Wyman-Changeux (MWC) model, in which low affinity T- and high affinity R- forms of enzymes coexist in a pre-equilibrium, independently of allosteric effectors (Monod et al., 1965). In order to get insights

into the behavior of *I. isl* MaDH, its crystal structure was solved and compared to relevant counterparts.

2.3. X-ray crystallography.

The crystal structure of *I. isl* MalDH was determined in the apo form. Data collection and refinement statistics are shown in **Table S1**. *I. isl* MalDH crystallizes in the space group $P22_12_1$ with a tetramer in the asymmetric unit. The tetrameric assembly corresponds to the oligomeric state determined in solution (**Fig. 1**). In three monomers, the electron density of an equivalent region corresponding to the mobile loop (residues 98 to 105, normalized numbering) was weak not allowing the corresponding residues to be modeled. The final tetrameric structure of *I. isl* MalDH is shown in **Fig. 3a**. Subunit contacts that maintain the tetramer state occur through interfaces along the P, Q and R axes.

As expected, the structure belongs to the NAD(P)-binding Rossmann-like Domain CATH superfamily (3.40.50.720, http://www.cathdb.info (Dawson et al., 2017). The *in silico* structural analysis made with the Superfamily server (Wilson et al., 2009) using the *I. isl* MaDH amino-acid sequence predicts two domains: a NAD(P)-binding Rossmann-fold domain (residues 7 to 138) and a LDH C-terminal-like domain (residues 146 to 308). When the *I. isl* MalDH structure is compared to all PDB content using the DALI server (http://ekhidna2.biocenter.helsinki.fi/dali/ (Holm and Laakso, 2016), the three highest scored structures correspond to two LDHs and one MalDH: *Metallosphaera sedula* MalDH (*M. sed* MalDH, Z=37.6, PDB ID: 6IHD, (Lee et al., 2019), *Plasmodium vivax* LDH (Z=36.8, PDB ID: 5HRU, (Choi and Ban, 2016) and *Lactobacillus casei* LDH (Z=36.2, PDB ID: 6J9T, http://dx.doi.org/10.2210/pdb6J9T/pdb).

In the following, the structural properties of *I. isl* MaDH are compared with homologs. These homologs were chosen on the basis of the fact that their biochemical properties have been established and their crystal structures also contain a tetramer in the asymmetric unit.

Structures of an allosteric LDH from *Thermus thermophilus* solved in both inactive and active states (*T. the* LDH, accession codes 2V6M and 2V7P) and the *Chlorobaculum tepidum* MalDH (*C. tep* MalDH, accession code 1GUZ) obey the previous criteria and were chosen as reference models for canonical LDH (in the two states) and MalDH respectively. Because of its strong similarity with *I. isl* MalDH, the enzyme from the crenarchaeon *M. sedula* was also taken into account.

As expected, the overall architecture of *I. isl* MaDH monomer is similar to all MalDHs and LDHs previously reported (**Fig. 3b**). However, the superposition reveals a noticeable difference. The α1G/α2G helix of each monomer is straight instead of kinked as observed in structures of homologs (**Fig. 3c**) with the exception of *Haloarcula marismortui* and *Haloferax volcanii* MalDHs structures (with respective accession codes 4JCO and 4BGU). In spite of its closest similarity with *I. isl* MalDH, *M. sed* MalDH has a kinked helix (not shown).

At a first glance, the quaternary assembly of *I.isl* MalDH contrasts to what has been observed with canonical tetrameric MalDHs and LDHs. This can be clearly observed thanks to a PyMOL superposition of the respective tetramers (**Fig. 3d**). The view through the bottom of the Q axis shows that AB-like dimer of *T. the* LDH and *C. tep* MalDH have almost the same arrangement. In contrast, when superimposed on other structures, the AB-like dimer of *I. isl* MalDH shows major secondary structure deviations around the Q axis, as well illustrated by its αH helix which moves away from equivalent position observed with its counterparts. The crystal structure of *I. isl* MalDH therefore corresponds to a new relative association between active dimers that make up the tetrameric assembly.

2.4. Solution structure of I. isl MalDH

To exclude that these structural particularities are due to a crystal packing bias, the structure of *I. isl* MalDH in solution was studied using SAXS (**Fig.4, Fig. S2 and Table S2**). A chimeric scattering curve was created by merging data from high and low concentration samples allowing to have access to small, middle and high angle data (**Fig. S2a**). Low angle

points were fitted using Guinier analysis; this indicated an absence of aggregates (**Fig. S2b**), and yielded a Rg of 3.28 nm (**Table S2**). The dimensionless Kratky plot, indicated that *I. isl* MalDH globally is not flexible (**Fig. S2c**). The analysis of the pair distance distribution function provided a value of Rg (3.16 nm) (**Table S2**) and a maximum distance found on the protein Dmax = 9 nm (Fig. S2d), similar to Dmax in the crystallographic structure (9.6 nm) (by taking into account the first hydration layer, Table S1). Also, the globular structure of *I. isl* MalDH is confirmed by the shape of the curve (**Fig. S2d**). The CRYSOL comparison between the theoretical curve calculated from the crystal structure and SAXS data shows a good agreement through the χ^2 value and visual inspection of the fit (Fig. 4). To confirm this, models of *I. isl* MalDH possessing the tetrameric assembly of canonical LDH and MalDH were produced by superposing a complete monomer of *I. isl* MalDH structure onto each monomer of *C. tep* MalDH and *T. the* LDH crystal structures. Poor fits were obtained with theoretical curves calculated from these models indicating that the canonical assembly does not explain the observed SAXS data (**Fig. S3a**). In fact, the crystal structure of *M. sed* MalDH reveals a similar tetrameric assembly as observed for *I. isl* MalDH. Again, a better fit is obtained when the *M. sed* MalDH model is used and then compared to models with a canonical tetrameric assembly (**Fig. S3b**).

This result demonstrates that the native state in solution is consistent with the novel relative association between dimers observed in the crystal structure of *I. isl* MalDH.

2.5. Comparison of the I. isl MalDH quaternary structure with homologs.

To go further in theses structural comparisons, other MalDH and LDH structures were superposed on *I. isl* MalDH using the program THESEUS (Theobald and Wuttke, 2006). RMSD values from the superposition between *C. tep* MalDH, *T. the* LDH (R- and T- states) and *M. sed* MalDH (in binary and ternary complex forms) with *I. isl* MalDH are reported on **Fig. 5a**.

Whereas RMSD values of the *I. isl* MalDH/*M. sed* MalDH quaternary assembly superposition are close to 1.5 Å, others are quite larger, indicating major structural differences, as revealed by the displacement vectors residue per residue shown in **Fig. 5** were generated using the modevector.py script from the PyMOLWiki website (http:// www.pymolwiki.org). When the I. isl MalDH was compared to canonical MalDH and LDH structures (**Figs 5b** and **Fig 5c**), main differences arose in the relative position of AB-like dimers. With the view along the Q-axis, an anticlockwise displacement of one active dimer relative to the other is observed. This quaternary structure corresponds to a new relative association of two active dimers leading to a more compact tetrameric assembly. Such a profound structural changes has rarely been described for closely related enzymes and mainly concerns those that display allosteric behavior (Singh et al., 2015; Barciszewski et al., 2016; Jiao et al., 2017).

The *I. isl* MalDH peculiar quaternary geometry relies on contact reorganization between subunits. An analysis of the interfaces of *I. isl* MalDH, *C. tep* MalDH and *T. the* LDH was made using PISA qt-interface (from the *CCP*4 suite (Winn et al., 2011**)**. Results are reported in **Table S3**. *I. isl* MalDH interface areas between monomers within AB-like dimers are almost in the same range as those of *C. tep* MalDH and *T. the* LDH in its T-state. In contrast, AD-like interface areas increase by approximatively 20%. These wider contact surfaces are consistent with the new tight association between dimers of dimers that make up the *I. isl* MalDH tetrameric assembly. The consequences of AD interface modification is analyzed in a section below. Thanks to a comparative study between large families of oligomeric proteins, it has been proposed that changes that lowered surfaces of contact between subunits in oligomeric proteins is a phenomenon favoring new pathways of evolution (Marsh and Teichmann, 2014). If true, it is tempting to propose that the compact tetrameric assembly observed with *I. isl* MalDH reflects the property of a new subgroup of enzymes, which i) either has followed a different evolutionary pathway within the superfamily of MalDHs and LDHs, ii) or represents the reminiscent state of an ancestral enzyme prior to the functional divergence. In the latter

case, the less compact assembly observed in canonical tetrameric MalDHs and LDHs might have been responsible for the emergence of their function and properties of regulation.

2.6. Structural basis of I. isl MalDH enzymatic properties

The enzyme was crystallized without co enzyme, so no comparison with respect to its binding mode is presented. Nevertheless, a structural comparison of several amino acids was performed with those found at equivalent position in LDHs and other tetrameric MalDHs (**Fig. S1** and **Fig. 6**). Indeed, numerous investigations using site-directed mutagenesis and crystallographic structures of MalDHs and LDHs have demonstrated that the nature of amino acid residues located at some key positions together with movements of some secondary structure elements are responsible for their different behavior (Clarke et al., 1986; Wilks et al., 1988; Cendrin et al., 1993; Iwata et al., 1994; González et al., 2018). Substrate binding and discrimination in LDHs and MalDHs are mainly due to four residues found at positions 102, 171, 199 and 246.

2.6.1. Positions 102, 199 and 246: Determinants of substrate discrimination.

The nature of amino acid at position 102, located on the mobile loop covering the catalytic site upon catalysis, is the main determinant of substrate discrimination between LDHs and MalDHs (Wilks et al., 1988; Cendrin et al., 1999; Boernke et al., 1995). It is always a glutamine and an arginine in canonical LDHs and MalDHs, respectively. Because of the high flexibility of the mobile loop, it was not modeled in three of the four monomers in the *I.isl* MalDH structure. However, in one monomer, a crystallization adjuvant interacts with the loop allowing the stabilization of an open position in which the lateral chain of Arg at position 102 is far away from the catalytic site and resembles the position found in most of the apo structures of MalDHs (not shown).

It is striking to observe that the *I. isl* MalDH sequence displays a Thr at position 246, whereas it is a residue typical of LDHs. In LDHs, the side chain of Thr246 through Van der Wall contacts participates to the correct orientation of the pyruvate during catalysis. The

superposition with the R- active state of *T.the* LDH (**Fig. 6a**) clearly shows that the lateral chain of Thr 246 in *I. isl* MaDH occupies an equivalent position. Mutagenesis experiments have demonstrated that Thr 246 selects against OAA recognition in LDHs (Wilks et al., 1988). In canonical MalDHs, the amino acid at position 246 is Ala or Ser; their tiny lateral chain allowing to accommodate OAA, which is larger than pyruvate. The structural comparison unambiguously shows the difference between *I. isl* MalDH and a canonical MalDH (**Fig. 6b**). The presence of a threonine at position 246 in *I. isl* MalDH may explain its capacity to also use pyruvate through an altered stringency of substrate discrimination.

The amino acid at position 199 is also involved in substrate discrimination between LDHs and MalDHs (Wilks et al., 1988). In LDHs, a negatively charged residue (Glu199) is always present and contributes to maintain the charge balance within the catalytic site upon catalysis (Wilks et al., 1988). In all MalDHs, there is a neutral residue at position 199, which is a methionine for most of the canonical MalDHs. In a molecular dynamics study using a canonical LDH-like MalDH from *Chlorobium vibrioforme*, it has been suggested, that Met199 plays a role in the conformational sampling of the mobile loop upon catalysis, by preventing non-productive interactions with the catalytic site (Kalimeri et al., 2014). In *I. isl* MalDH, there is also a neutral residue, but it is an alanine instead of a methionine (**Fig. 6b**). Primary sequence inspection of MalDHs from *crenarchaeota* indicates that alanine at position 199 is conserved for this phylum. This may suggest that MalDHs from *crenarchaeota,* including *I. isl* MalDH, display specific dynamical properties compared to canonical tetrameric MalDHs.

2.6.2. Position 171: Main substrate binding residue

In canonical LDHs and MalDHs, Arg171 is the universally conserved substrate binding residue (Madern, 2002). The amine moiety of Arg171 lateral chain interacts with the carboxylate moiety shared by both pyruvate and oxaloacetate substrate. In allosteric *T. the* LDH, R171 can adopt two different conformations, being either outside or inside the active site in the T- inactive and R- active state representative structures, respectively (Colletier et al., 2012). These conformations are labelled as cs-out and cs-in (**Fig. 6**). Comparison of the position of Arg171 in *I. isl* MalDH structure with the ones in *T. the* LDH illustrates it occupies

an intermediate position (**Fig. 6a-d**). The comparison shows part of the lateral chain is in a position which rather mimics the Arg171-cs-in conformation than the Arg171-cs-out one of an allosteric LDH, with the NH_2 extremity exploring a new conformational sub state (**Fig. 6a-d**). This peculiar position was unambiguously modeled in all *I. isl* MalDH monomers (**Fig. S4**) and thus corresponds to a new angular position described for the first time in enzymes of the superfamily. Comparisons with *C. tep* MalDH taken as canonical tetrameric MalDHs, and with the recently solved *crenarchaeal* MalDH from *M. sedula* confirm the new position of Arg171 is a specific feature of *I .isl* MalDH (compare **Fig. 6c-e**).

Because the NH_2 extremity does not completely protrude within the catalytic site, it could be considered as a non-productive conformational sub-state, different from the one observed within the T- inactive state of LDH. The sigmoid activity profile when pyruvate was used as substrate suggested that *I. isl* MalDH in solution may explore inactive and active states; the peculiar local topology of R171 observed in the apo structure represents an inactive state of *I. isl* MalDH.

2.7. A tentative explanation of Arg171 conformation in I. isl MalDH

Several reasons can explain the peculiar position of Arg171 in *I. isl* MalDH.

The first concerns the specific topology of α1G-α2G helix, which is straight and consequently slightly changes the catalytic site local topology allowing the lateral chain of Arg171 to acquire a higher degree of flexibility. This is illustrated by the comparison of *I. isl* MalDH (**Fig. 7a**) with *C. tep* and *M. sed* MalDHs (**Fig. 7b-c**) showing that the presence of a kinked helix α1G-α2G induces stearic contacts, which restrict the capacity of Arg171 in the latter enzymes to explore a wider conformational space.

The second reason is related to the presence of a histidine at position 68 in *I. isl* MalDH, whereas it is typical residue of allosteric LDHs (Otha et al., 1992). In most canonical tetrameric MalDHs, as illustrated in *C. tep* MalDH, the arginine side chain is strongly maintained within the active site by a stabilizing salt bridge with Asp68 from the adjacent monomer B (**Fig. 6c**). In the *T. the* LDH structure (**Fig. 6b-d**), His68 from monomer B and Arg171 are adjacent

residues with coordinated side chain conformations (Coquelle et al., 2007; Colletier et al., 2012). When His68 is in the conformation observed in the T- inactive state, it prevents the side chain of Arg171 from accessing the active site (cs-out) and adopting the R- state conformation that binds the substrate analog, oxamate. In *I. isl* MalDH, the His68 conformation corresponds to the conformer observed with *T. the* LDH in its R- active state, an observation that explains why Arg171 side chain is located within the catalytic site (**Fig. 6b**). This explanation holds also for *M. sed* MalDH (**Fig. 6e**).

Comparison of *I. isl* MalDH structure with canonical LDHs and MalDHs, reveals a third reason that impacts the Arg171 local dynamics in *I. isl* MalDH. In *T. the* LDHs, a large region (residues 168-232) was considered as a mobile core located at the AD interface (P axis-subunit interface) and was proposed to couple local motions within the core to the quaternary structural changes associated with allostery (Taguschi, 2017 and references therein). Mutations that target this core region in LDHs from different *Thermus* species were shown to strongly influence their allosteric properties by changing substrate affinity thanks to long range distance effects (Colletier et al., 2012, Ikehara et al., 2014). Arg171 and its neighboring amino acid Phe172 belong to this mobile core. In the *I. isl* MalDH equivalent region, the side chain of Phe172 is inward-oriented (**Fig. 8**). It interacts with the bulky side chain of Trp203 and Val201, making a packed hydrophobic environment, very similar to the one observed in *T. the* LDH that possess a conserved tryptophan and a leucine at positions 203 and 201, respectively. In contrast, in *C. tep* MalDH, there is a proline and a valine at position 201 and 203, respectively. The decrease in the local packing density may contribute to prevent allosteric communication within the quaternary assembly of MalDHs.

As a result of the comparison, it is clear that the substrate binding residue of *I. isl* MalDH is in a local environment similar to the one in LDH.

2.8. Conformational organization of the catalytic center in I. isl MalDH

The reactions catalyzed by LDHs and MalDHs are similar. They involve the direct transfer of a hydride ion from the reduced state of NADH to pyruvate or oxaloacetate,

accompanied by the protonation of substrates' keto oxygen (Holbrook et al., 1975). The proton is provided by the universally conserved histidine 195. Within the active site, His195 is polarized thanks to its interaction with Asp168 (Birktoft & Banaszak, 1983). Moreover, in LDHs there is always a glutamic acid at position 194, which may form transient interactions with the universally conserved Arg109 hold on the catalytic mobile loop. In *I. isl* MalDH, the local orientations of His195, involved in the His-Asp proton relay system, and of Glu194 resemble the ones of an LDH rather than that of a MalDH (**Fig. 9a**). The superposition of three other tetrameric MalDHs structures (1GUY, 4BVG and 5ULV), confirms that the His195 orientation is totally different (**Fig. 9b**), which may be associated with the absence of Glu194 (replaced by a glycine).

To conclude, both the nature and local properties of key amino acids located with the catalytic site of *I. isl* MalDH in its apo state are likely to establish interactions involved in conformational organization of the catalytic center as observed in LDHs rather than in MalDHs.

2.9. Structural organization of the putative allosteric core in I. isl MalDH.

The other structural features that define *I. isl* MalDH as an enzyme with intermediate properties between allosteric LDHs and non-allosteric tetrameric MalDHs concern two helices (α2F and αT). In LDHs, these have been described as being parts of the mobile core, which couples structural changes at the AD-like interface during the allosteric transition (49 and references therein). During the allosteric transition, helix α2F moves by 15° allowing the lateral chain of R171 to enter the catalytic site (Iwata et al., 1994) and this displacement is accompanied by the movement of helix αT, as can be observed by comparing the *T. the* structures in the R- and T- states (**Fig. 6b-c**).

Again, the structure of *I. isl* MalDH resembles that of canonical LDHs. First, it is remarkable to observe that αT helix in *I. isl* MalDH has a size similar to the one observed in LDHs (**Fig. 6**). Then, helix α2F superimposes well with its counterpart of the R- active state of *T. the* LDH (**Fig. 6b**), but not helix αT (**Fig. 6b**). The opposite is observed when compared to

the T- inactive state of *T. the* LDH (**Fig. 6d**). Thus, positions of α2F and αT helices in *I. isl* MalDH are a mix of the positions observed in the two states of canonical allosteric LDH.

2.10. I. isl MalDH quaternary assembly prevents FBP binding sites formation

At this stage of the comparative analysis of *I. isl* MalDH, which has revealed a closer relationship with allosteric LDHs, the absence of heterotropic activation by FBP should be clarified. In allosteric LDHs, two FBP molecules are bound at the AD-like interface between active dimers where Arg173, His188 and Tyr190 of two juxtaposed subunits interact with the two phosphate groups of FBP (Iwata et al., 1994). Primary sequence inspection of *I. isl* MalDH showed that both Arg and Tyr are conserved with the exception of an Asp residue instead of His at position 188 (**Fig. S1**). Even without any knowledge of the structure, the presence of a negatively charged residue was expected to prevent FBP binding because of a charge repulsion effect. Furthermore, the peculiar quaternary geometry of *I. isl* MalDH prevents the formation of an appropriate FBP-binding site topology by dramatically increasing the distance between the various amino acid residues involved in the site (**Fig. 10**). So that, neither the amino sequence of putative allosteric effector-binding site, nor the suitable topology allowing FBP-binding site formation are achieved in *I. isl* MalDH; despite its close resemblance with allosteric LDHs.

2.11. Hidden homotropic activation in I. isl MalDH

As expected, the *I. isl* MalDH behaves as a Michaelian enzyme with its natural substrate OAA. However, the enzymatic activity profile showing a sigmoid activation by pyruvate has revealed that *I. isl* MalDH has an intrinsic hidden homotropic allosteric capacity. In the recent framework of allostery, the capacity to behave as an inactive or active state for an allosteric enzyme is mainly due to a population shift among preexisting conformers (Motlagh et al., 2014), with some displaying hidden allosteric properties, such as analyzed using the PDZ3 domain protein (Kumawat and Chakrabarty, 2017). It has been proposed that intrinsic allostery may be hidden under some conditions and triggered under other circumstances (Kumawat and Chakrabarty,

2017). In particular, it has been shown that a single mutation could be effective to unmask this phenomenon (Hegazy et al., 2013). Several works have shown allostery is a dynamical phenomenon which does not necessarily imply a major structural rearrangement to modify protein properties, side chains dynamics being sufficient enough to propagate redistribution of energy within a protein (Nussinov and Tsai, 2015; Kumawat and Chakrabarty, 2017). The *I. isl* MalDH behavior fits this general framework. It exhibits local structural changes different from those existing in other MalDHs that might favor its hidden allosteric behavior. Further site-directed mutagenesis experiments are needed to decipher how the fine interplay between the role of LDH-specific residues in *I. isl* MalDH and those which control quaternary assembly impact its intrinsic allostery.

3. Conclusions and evolutionary considerations

The present work established that *I. isl* MalDH possesses clear malate dehydrogenase activity. However, it is also able to use pyruvate as substrate and is sensitive to homotropic activation, a phenomenon specific of allosteric LDH. In virtue of its crystal structure, this unexpected characteristic is related to the presence, at key positions, of amino acids generally found in LDHs. Surprisingly, the *I. isl* MalDH structure revealed a new organization of the tetrameric state. The peculiar biochemical and structural properties of *I. isl* MalDH therefore raises the question of its evolutionary relationship within the MalDH/LDH superfamily.

The most convincing, and still prevailing scenario to explain molecular evolution within the superfamily states that canonical LDHs were selected from an ancient gene duplication with tetrameric LDH-like MalDHs (Madern, 2002). Further gene duplications and neofunctionalisation have led to the convergent selection of LDH function from recent LDH-like MalDHs, in particular with apicomplexa (Madern et al., 2004; Boucher et al., 2014). It should be emphasized that the other mitochondrial and cytosolic dimeric MalDHs clades have a more distant phylogenetic relationship with LDHs (Madern, 2002). Following the present work, it is possible to make the hypothesis that archaeal LDH-like MalDHs, in particular (or including) those from the *crenarchaeota* phylum, are more closely related to LDHs than

bacterial LDH-like MalDHs. Our results are in strong agreement with an enzyme evolution hypothesis, which states that conformational diversity and functional promiscuity are strong drivers of protein evolution (James and Tawfik, 2003). In such a framework, *I. isl* LDH-like MalDH might be considered as one of the closest relatives of an ancestral enzyme that displayed i) a promiscuous capacity of substrate recognition, ii) a pre-allosteric capacity and iii) a compact tetrameric state. After the duplication of such an ancestral gene, the resulting copies were prone to evolve new functions and regulations. Following amino acids substitutions that arose during evolution, some of the ancestral state properties would either have been unlocked and amplified or abolished in the different groups of enzymes in the super family.

4. Materials and methods

4.1. Cloning of I. isl MalDH.

A gene encoding the malate dehydrogenase of *I. islandicus* with codons optimized for expression in E. coli was synthetized and subcloned into pET-20a by Gencust. The NdeI and BamHI cloning sites were used for cloning.

4.2. Protein expression and purification.

E. coli BL21 DE competent cells transformed with pET-20 expression vector encoding *I. isl* MalDH gene were selected by growth on LB agar plates containing 100 µg ml^{-1} ampicillin. A single colony was grown overnight at 37°C in 50 ml^{-1} LB medium at the same concentration of antibiotic. 20 ml^{-1} of these cultures were then used for inoculation of a 2 liter LB medium containing 100 µg ml^{-1} ampicillin. The cells were cultivated at 37°C until an OD_{600} of 0.6 was reached. Isopropyl B-D-1-thiogalactopyranoside (IPTG) was added at a final concentration of 0.5 mM to induce expression and the culture was incubated for 4 hours at 37°C. Bacterial cells were harvested by centrifugation at 6000 g for 20 minutes at 4°C. The pellet was suspended in 40 mL of 50 mM Tris-HCl pH 7.4 containing 50 mM NaCl (Buffer A). Prior cell disruption, 5

µg ml^{-1} of DNAse and $MgCl_2$ to final concentration of 15 mM was added to the cell suspension. The preparation was cooled at 4°C and lysed by sonication (Branson sonicator). Six cycles of continuous sonication at 50 % amplitude were applied during 30 s. Between each pulse, the solution was kept on ice for one minute. The extract was then centrifuged at 13000 g for 30 min at 4°C. The supernatant was further incubated at 70°C for 30 min and the thermally unfolded proteins were removed by centrifugation. The extract was loaded on a Q sepharose column (2x10 cm) equilibrated with Buffer A. *I. isl* MalDH was eluted with a linear gradient from 0 to 0.8 M NaCl in Buffer A. The active fractions containing the enzyme were pooled, concentrated and loaded on a Superpose 12 gel-filtration column (GE Healthcare) and eluted with Buffer A. The purity of the enzyme was checked by SDS gel electrophoresis. The enzyme was concentrated at 20 mg ml^{-1} in Buffer A and stored at 4°C.

4.3. Size Exclusion Chromatography - Multi Angle Laser Light scattering (SEC-MALLS)

SEC combined with online detection by MALLS and refractometry (RI) was used to measure the absolute molecular mass of *I. isl* MalDH in solution. The SEC run was performed using an ENrich™ SEC650 10x300 gel-filtration column (Biorad) equilibrated with a buffer composed of 50 mM Tris-HCl pH7.2 and 50 mM NaCl. Separation was performed at room temperature and 50 µl of protein sample, concentrated at ~5 mg ml^{-1}, was injected with a constant flow rate of 0.5 ml^{-1} min^{-1}. Online MALLS detection was performed with a DAWN-HELEOS II detector (Wyatt Technology Corp.) using a laser emitting at 690 nm. Protein concentration was determined by measuring the differential refractive index online using an Optilab T-rEX detector (Wyatt Technology Corp.) with a refractive index increment *dn/dc* of 0.185 ml^{-1} g^{-1}. Weight-averaged molecula weight (Mw) determination was done with the ASTRA6 software (Wyatt Technologies) and curve was represented with GraphPad Prism.

4.4. Enzymatic assay and protein determination

The activity of *I. isl* MalDH for reduction of oxaloacetate to malate was carried out at 70°C in 500 µL of 50 mM phosphate buffer pH 7.0 containing 50 mM NaCl. Assays using

pyruvate as substrate were done in 500 µL of 2-(N-morpholino) ethane sulfonic acid (MES) pH 6.0 and supplemented with 50 mM NaCl. The reaction was monitored spectrophotometrically at 340 nm by following the oxidation of NADH (0.5mM) on a Jasco 540. To record the enzymatic profile of *I. isl* MalDH, various substrate concentrations were tested. The data were analyzed using Michaelis-Menten or allosteric sigmoidal equations in GraphPad Prism version 7.03. The protein concentration was estimated from the absorbance at 280 nm using a nanodrop Thermofischer. The server https://web.expasy.org/protparam/ (Gasteiger et al., 2005) was used to compute a molecular weight of 33.5 and a theoretical extinction coefficient of 21430 M^{-1} cm^{-1}.

4.5. Crystallization and structure determination

I. isl MalDH was crystallized by vapor diffusion using the sitting drop method at 293 K (HTXLab, CRIMS©). The Tb-Xo4 crystallophore™ (Engilberge et al., 2017, Engilberge et al., 2018) was added to the 4 mg ml^{-1} protein solution at a 10 mM final concentration. The crystals were grown in 2 days by mixing 1 µL of the protein solution with 1 µL of 10% PEG 6000 and 100 mM Hepes at pH 7 reservoir solution. No supplementary cryoprotection was needed. The crystals were harvested directly to the drop and flash-frozen in liquid nitrogen.

I. isl MalDH diffraction data were collected on the Proxima-1 beamline at the synchrotron radiation source SOLEIL (Gif-sur-Yvette, France). Datasets were indexed and integrated using XDS (Kabsch, 2010). Scaling, density modification and molecular replacement were done with the CPP4 suite using SCALA (Evans, 2006), DM (Cowtan, 1999) and PHASER (McCoy et al., 2007). The model used for molecular replacement was the structure of *Haloferax volcanii* MalDH (RCSB PDB accession code: 4BGU). The structure was refined with multiple cycles of manual building using COOT (Emsley et al., 2010) and of refinement using phenix.refine (PHENIX suite, Afonine et al., 2012) and BUSTER (https://www.globalphasing.com/buster). The NCS option was not used to avoid symmetric bias. The TLSMD server (http://skuld.bmsc.washington.edu/~tlsmd/ (Painter and Merritt, 2005;

Painter and Merritt, 2006) was used to generate TLS groups. Model quality was validated with MolProbity (http://molprobity.biochem.duke.edu), (Davis et al., 2007; Chen et al., 2010) and wwPDB validation service (https://validate-rcsb-1.wwpdb.org), (Berman et al., 2003). The table of data collection and refinement statistics was obtained using phenix.table-one (PHENIX suite). Surface analyses performed using PISA Qt-interface (CCP4, (Krissinel, 2015).

4.6. SAXS experiments

SAXS experiments were performed at the European Synchrotron Radiation Facility (ESRF) on the beamLine BM29 "BioSAXS" using an X-ray wavelength of 1.25 Å and a sample distance from the detector of 2.85 m. I*. isl* MalDH data were collected at 0.39, 1.68, 4.45, 6.1 and 9.31 mg ml^{-1} in the scattering vector range from 0.003 to 0.494 $Å^{-1}$. Buffer solution scattering curves were recorded before and after each protein sample. To prevent radiation damage, each measurement has been made 10 times and then averaged. Sample scattering curves were obtained after subtraction of the averaged buffer signals using standard protocols with PRIMUS (Konarev et al., 2003). The chimera scattering curve, used for the rest of the analysis, was created from a low (0.39 mg ml^{-1}) and a high concentration (9.31 mg ml^{-1}) sample scattering curve. The Rg, I(0) and D_{max} values were obtained with Primus Guinier Wizard and Primus Distance Distribution Wizard. The model of *I. isl* MalDH based on the crystal structure and completed with the four mobile loops has been compared to SAXS data with CRYSOL (Svergun et al., 1995). The maximum s value was limited to 0.3 Å to avoid a fit with too noisy data.

4.7. Primary sequence alignment, structural superpositions and representations

Primary sequences were aligned using MUSCLE (Edgar, 2004).

To perform homogeneous comparisons between PDB files, chains were renamed according to MalDH and LDH standards, as monomers A, B, C and D, respectively located at upper left, upper right, down right and down left positions.

Structural superpositions of the *I. isl* MalDH crystal structure onto canonical MalDH and LDH structures were made using THESEUS (Theobald and Wuttke, 2008; Theobald and Steindel, 2012) The MalDH of *Chlorobaculum tepidum* (PDB ID: 1GUZ, (Dalhus et al., 2002)), R-state (PDB ID: 2V6M) and T-state (PDB ID: 2V7P) of the LDH of *Thermus thermophilus* (Coquelle et al., 2007) were selected. These model structures were chosen depending on their high resolution and tetrameric fold. In the case of *C. tep* MalDH, the structure was solved as a binary complex with NADH, however this binding does not induce significant structural reorganization in tetrameric MalDHs as shown by González et al. (2018). To base the superposition work only on C-alpha structures, polyGLY models were set up with PDBCUR and PDBSET from CCP4. The structure images were represented with PyMOL (The PyMOL Molecular Graphics System, Version 1.8.6.0 Schrödinger, LLC).

Acknowledgements

The authors acknowledge Drs Céline Armanet-Brochier, Frank Gabel, Jacques Coves and for helpful discussions and Giuseppe Zaccai for a critical reading of the manuscript. The authors also acknowledge funding by Agence Nationale de la Recherche (ANR) grant to DM (program AlloAnc ANR-16-CE11-0011) and to EG (program Ln23 ANR-13-BS07-0007-01). This work used the platforms of the Grenoble Instruct center (ISBG; UMS 3518 CNRS-CEA-UJF-EMBL) with support from FRISBI (ANR-10-INSB-05-02) and GRAL (ANR-10-LABX-49-01) within the Grenoble Partnership for Structural Biology (PSB)

Conflict of interest

The authors declare that they have no conflicts of interest with the contents of this article.

Author contributions

DM conceived the project. DM performed sample preparation and enzymatic measurements, CM performed MALLS experiments, JR performed the SAXS experiments, conducted crystallization trials, diffraction data collection and structure refinement. EG contributed to diffraction data collection and structure refinement. All the authors analyzed data, discussed the data and wrote the paper.

Accession numbers

Accession number PDB ID for *I. isl* MalDH structure: 6QSS. Accession number SASBDB ID for *I. isl* MalDH: SASDF93.

Figure legends

Fig. 1. SEC-MALLS analysis of *I. isl* MalDH in solution. The chromatogram shows the elution profile monitored by excess refractive index (left ordinate axis) and the molecular weight as dashed line (right ordinate axis) derived from MALLS and refractometry measurements. The estimated average molecular weight is indicated on the graph.

Fig. 2. Enzymatic activity profiles of *I. isl* MalDH. Reaction velocities were measured in the presence of the indicated concentrations of substrate. (A) Oxaloacetate. (B) Pyruvate.

Fig. 3. Structure of the apo form of tetrameric *I. isl* MalDH. (A) Cartoon representation of the four monomers are labeled A to D. Chains are colored in "chainbow" mode. Subunits of the tetrameric assembly are related by three molecular dyads, *P*, *Q* and *R*. (B) *I. isl* MalDH monomer representation. α-helices are colored in orange whereas β-strands and loops are in green and red, respectively. Secondary structures are labeled according to the LDH structure Coquelle et al., 2007). (C) Superposition using PyMOL of the monomer of *I. isl* MalDH structure with *C. tep* MalDH (1GUZ) and *T. the* LDH structures (2V6M), respectively. *I. isl* MalDH, *C. tep* MalDH and *T. the* LDH structures are colored respectively in red, purple blue and deep olive. The close-up view is centered on α1G/α2G helices. (D) PyMOL superposition between AB-like dimer of *I. isl* MalDH and its counterparts. The view is through the *Q* axis bottom. The red label corresponds to *I. isl* MalDH secondary structure whereas black corresponds to the other structures.

Fig. 4. *I. isl* MalDH SAXS/X-ray crystallography comparison using CRYSOL from the ATSAS suite. SAXS experimental data are represented by red dots. SAXS theoretical data calculated from an atomic model of the crystallographic structure completed with the four mobile loops are reported as a green curve.

Fig. 5. Structure superpositions calculated with THESEUS and represented using the PyMOL modevectors script. (A) RMSD values resulting from THESEUS superpositions of the tetramers. (B) Superposition of a canonical MalDH structure (1GUZ) to *I. isl* MalDH structure. (C) Superposition of a canonical LDH structure (2V6M) to *I. isl* MalDH structure. Top and bottom parts of the figure correspond to a view along the R and Q axis, respectively.

Fig. 6. Close-up views showing pairwise comparison of the *I. isl* MalDH catalytic site with homologs. *I. isl* MalDH is colored in red. Numbering as explained in the main body of the text. (A) Amino acid differences at equivalent position as discussed in the main text. Most of them are shown as sticks in the others panels. Helix αC from adjacent monomer is always colored in salmon and indicated with a star. Cs-in and cs-out refer to the two conformational sub-states of Arg171, inside or outside the catalytic site, respectively. (B) Comparison of *I. isl* MalDH with the R- state (2V7P) of *T. the* LDH (brown), substrate analog oxamate is shown in green. (C) Comparison with *C. tep* MalDH (1GUZ) (purple marine). (D) Comparison of *I. isl* MalDH with the T- state (2V6M) of *T. the* LDH (deep olive). (E) Comparison with *M. sed* MalDH (6IHD) (cyan).

Fig. 7. Close-up views of the universally conserved substrate binding Arg171 lateral chain positions (LDH nomenclature) and neighboring residues located on α1G/α2G helix in different MalDHs. (A) *I. isl* MalDH. (B) *C. tep* MalDH (1GUZ). (C) *M. sed* MalDH (6IHD).

Fig. 8. Close-up views of the putative allosteric core. Residues at equivalent positions according to LDH nomenclature are represented as sticks. To illustrate contacts between residues, the van der Wall surface is depicted for some of them. (A) *T. the* LDH (2V7P). (B) *I. isl* MalDH. (C) *C. tep* MalDH.

Fig. 9. Close-up views of the catalytic histidine H195. (A) Superposition of *I. isl* MalDH with *T. the* LDH (2V7P), colored in red and grey respectively. (B) Superposition between three

different MalDHs from *Chloroflexus aurantiacus*, *Picrophilus torridus* and *Methylobacterium extorquens* (PBD accession code: 1GUY, 4BGV and 5ULV)

Fig. 10. Close-up view of the AD-like dimer. In each monomer, helix α2F is represented in ribbon. For the sake of clarity most part of the structures is not drawn. Important residues involved in FBP binding are show as sticks at positions 173, 188 and 190. (A) FBP-binding site of *T. the* LDH (2V7P). Because the enzyme was not crystallized with the allosteric effector, the FBP molecule (yellow dots) that is shown comes from the superimposition with *Bifidobacterium longum* LDH structure (1LTH). Ribbon drawing of the latter enzyme is masked. (B) Putative binding site in *I. isl* MalDH. Because of the new geometry, helix α2F of monomer D, has changed its relative orientation.

Table 1. Kinetic properties of *I. isl* MalDH.

References

Afonine, P. V., Grosse-Kunstleve, R. W., Echols, N., Headd, J. J., Moriarty, N. W., Mustyakimov, M., Terwilliger, T. C., Urzhumtsev, A., Zwart, P. H., Adams, PD. (2012). Towards automated crystallographic structure refinement with phenix.refine. Acta Cryst. D. 68, 352-367.

Arai, K., Ichikawa, J., Nonaka, S., Miyanaga, A., Uchikoba, H., Fushinobu, S., Taguchi, H. (2011). A molecular design that stabilizes active state in bacterial allosteric l-lactate dehydrogenases. J Biochem. 150, 579-591.

Barciszewski, J., Wisniewski, J., Kolodziejczyk, R., Jaskolski, M., Rakus, D., Dzugaj, A. (2016). T-to-R switch of muscle fructose-1, 6-bisphosphatase involves fundamental changes of secondary and quaternary structure. Acta Cryst. D 72, 536-5300

Berman, H., Henrick, K., Nakamura, H. (2003). Announcing the worldwide Protein Data Bank. Nature Struct. Mol. Biol. 10, 980-980.

Birkoft, J. J. Fernley, R. T., Bradshaw, R. A., Banaszak L. J. (1982). Amino acid sequence homology among the 2-hydroxyacid dehydrogenase, mitochondrial and cytoplasmique malate dehydrogenase form a homologous system with lactate dehydrogenase. Proc. Natl. Acad. Sci. USA 79, 6166-6170.

Birktoft, J. J., Banaszak, L. J. (1983). The presence of a histidine-aspartic acid pair in the active site of 2-hydroxyacid dehydrogenases. X-ray refinement of cytoplasmic malate dehydrogenase. J. Biol. Chem. 258, 472-482.

Boernke, W. E., Sanville-Millard, C., Wilkins-Stevens, P., Kakar, S. N., Stevens, F. J., Donnelly, M.I. (1995). Stringency of substrate specificity of *Escherichia coli* malate dehydrogenase. Arch. Biochem. Biophys. 332, 43-52.

Boucher, J. I., Jacobowitz, J. R., Beckett, B. C., Classen, S., Theobald, D. L. (2014). An atomic-resolution view of neofunctionalization in the evolution of apicomplexan lactate dehydrogenases. ELife 3.

Burgner, J. W., Ray, W. J. (1984). On the origin of lactate dehydrogenase induced rate effect. Biochemistry 23, 3636-3648.

Cendrin, F., Chroboczek, J., Zaccai, G., Eisenberg, H.,Mevarech, M. (1993). Cloning, sequencing and expression in *Escherischia coli* of the gene coding for malate dehydrogenase of the extremely halophilic archaebacterium *Haloarcula marismortui*. Biochemistry 32, 4308-4313.

Chapman, A. D., Cortes, A., Dafforn, T. R., Clarke, A. R.,Brady, R L. (1999). Structural basis of substrate specificity in malate dehydrogenases, crystal structure of a ternary complex of porcine cytoplasmic malate dehydrogenase, alpha-ketomalonate and tetrahydoNAD. J. Mol. Biol. 285, 703-712.

Chen, V.B., Arendall, W. B., Headd, J.J., Keedy, D. A., Immormino, R. M., Kapral, G. J. Murray, L. W., Richardson, J. S., Richardson, DC. (2010). *MolProbity*, all-atom structure validation for macromolecular crystallography. Acta Cryst. D. 66, 12-21.

Choi, S. J., Ban, C. (2016). Crystal structure of a DNA aptamer bound to PvLDH elucidates novel single-stranded DNA structural elements for folding and recognition. Sci Rep 6, 34998.

Clarke, A. R., Wigley, D. B., Chia, W. N., Barstow, D., Atkinson, T., Holbrook J. J. (1986). Site-directed mutagenesis reveals role of mobile arginine residue in lactate dehydrogenase catalysis. Nature. 324, 699-702.

Clarke, A. R., Wilks, H. M., Barstow, D. A., Atkinson, T., Chia, W. N., Holbrook, J. J. (1988). An investigation of the contribution made by the carboxylate group of an active site histidine-aspartate couple to binding and catalysis in lactate dehydrogenase. Biochemistry 27, 1617-1622.

Colletier, J. P., Aleksandrov, A., Coquelle, N., Mraihi, S., Mendoza-Barberá, E., Field, M., Madern, D. (2012). Sampling the conformational energy landscape of a hyperthermophilic protein by engineering key substitution. Mol. Biol. Evol. 29, 1683-1694.

Coquelle, N., Fioravanti, E., Weik, M., Vellieux, F., Madern, D. (2007). Activity, Stability and Structural Studies of Lactate Dehydrogenases Adapted to Extreme Thermal Environments. J. Mol Biol. 374, 547–562.

Cowtan, K. (1999). Error estimation and bias correction in phase-improvement calculations. Acta Cryst. D. 55, 1555-1567.

Dalhus, B., Saarinen, M., Sauer, U. H., Eklund, P., Johansson, K., Karlsson, A., Ramaswamy, S., Bjørk, A., Synstad, B., Naterstad, K., Sirevåg, R., Eklund, H. (2002). Structural Basis for Thermophilic Protein Stability, Structures of Thermophilic and Mesophilic Malate Dehydrogenases. J. Mol. Biol. 318, 707-721.

Davis, I. W., Leaver-Fay, A., Chen, V.B., Block, J. N., Kapral, G. J., Wang, X., Murray, L. W. Arendall, W. B., Snoeyink, J., Richardson, J. S., Richardson, D. C. (2007). MolProbity, all-atom contacts and structure validation for proteins and nucleic acids. Nucleic Acids Res 35, 375-38366.

Dawson, N. L., Lewis, T. E., Das, S., Lees, J. G., Lee, D., Ashford, P., Orengo, C. A., Sillitoe, I. (2017). CATH, an expanded resource to predict protein function through structure and sequence. Nucl. Ac. Res. 45, 289-295.

Edgar, R. C (2004). MUSCLE multiple sequence alignment with high accuracy and high throughtput. Nucleic Acid. Res. 32, 1792-1797.

Emsley, P., Lohkamp, B., Scott, W. G., Cowtan, K. (2010). Features and development of Coot. Acta Cryst. D. 66, 486-501.

Engilberge, S., Riobé, F., Wagner, T., Pietro, S.D., Breyton, C., Franzetti, B., Shima, S., Girard, E., Dumont, E., Maury, O. (2018). Unveiling the Binding Modes of the Crystallophore, a Terbium-based Nucleating and Phasing Molecular Agent for Protein Crystallography. Chemistry. 24, 9739-9746.

Engilberge, S., S., Riobé, F., Di Pietro, S., Lassalle, L., Coquelle, N., Arnaud, C. A., Pitrat, D. , Mulatier, J. C., Madern, D., Breyton, C., Maury, O., Girard, E. (2017). Crystallophore, a versatile lanthanide complex for protein crystallography combining nucleating effects, phasing properties, and luminescence. Chem Sci 8, 5909–5917.

Evans, P. (2006). Scaling and assessment of data quality. Acta Cryst. D. 62, 72-82.

Eventoff, W., Rossmann, M. G.,Taylor, S. S., Torff, H. J., Meyer, H., Keil, W., Kiltz, H. H. (1977). Structural adaptations of lactate dehydrogenase isozymes. Proc. Natl. Acad. Sci. USA 74, 2677-2268.

Ferst, A. (1985). Enzyme structure and mechanism, 2nd edition freeman and Co., New york.

Gasteiger, E., Hoogland, C., Gattiker, A., Duvaud, S., Wilkins, M. R., Appel, R. D. , Bairoch, A. (2005). Protein Identification and Analysis Tools on the ExPASy Server, In Walker, JM (eds), The Proteomics Protocols Handbook. , p 571, Humana, Totowa, NJ.

González, J. M., Marti-Arbona, R., Chen, J. C. H., Broom-Peltz, B., Unkefer, C. J. (2018). Conformational changes on substrate binding revealed by structures of Methylobacterium extorquens malate dehydrogenase. Acta Crys. F 74, 610–616.

Harms, M. J., Thornton, J. W. (2010). Analyzing protein structure and function using ancestral gene reconstruction. Curr. Opin. Struct. Biol. 20, 360-366.

Hart, K. W., Clarke, A. R., Wigley, D. B., Chia, W. N., Barstow, D. A., Atkinson, T., Holbrook, J. J. (1987). The importance of arginine 171 in substrate binding by *Bacillus stearothermophilus* lactate dehydrogenase. Bio. Bioph. Res. Com. 146, 346–353.

Hart, K. W., Clarke, A. R., Wigley, D. B., Waldman, A. D. B., Chia, W. N., Barstow, D. A., Atkinson, T., Jones, J. B., Holbrook, J. J. (1987). A strong carboxylate-arginine interaction is important in substrate orientation and recognition in lactate dehydrogenase. B. B. A. 914, 294-298.

Hartl, T., Grossebüter, W., Görisch, H., Stezowski, J. J. (1987). Crystalline NAD/NADP-Dependent Malate Dehydrogenase; the Enzyme from the Thermoacidophilic Archaebacterium Sulfolobus acidocaldarius. Biol Chem Hoppe Seyler. 368, 259-267.

Hegazy, U. M., Musdal, Y., Mannervik, B. (2013). Hidden allostery in human glutathione transferase P1-1 unveiled by unnatural amino acids substitutions and inhibitions studies. J. Mol. Biol. 425, 1509-1514.

Holbrook, J. J., Liljas, A., Steindel, S. J., Rossmann, M. G. (1975) Lactate Dehydrogenase. In Boyer, PD (ed), pp. 191, The Enzymes. Academic Press, London.

Holm, L., Laakso, L. M. (2016). Dali server update. Nucl. Ac. Res. 44, 351-355.

Ikehara, Y., Arai, K., Furukawa, N., Ohno, T., Miyake, T., Fushinobu, S., Nakajima, M., Miyanaga, A., Taguchi, H. (2014). The Core of Allosteric Motion in *Thermus caldophilus* l-Lactate Dehydrogenase. J. Biol. Chem. 289, 31550-31564.

Irimia, A., Ebel, C., Madern, D;, Richard, S. B., Cosenza, L. W., Zaccai, G., Vellieux, F. M. (2003). The Oligomeric states of Haloarcula marismortui malate dehydrogenase are modulated by solvent components as shown by crystallographic and biochemical studies. J. Mol. Biol. 326, 859-873.

Iwata, S., Kamata, K., Yoshida, S., Minowa, T., Ohta, T. (1994). T and R states in the crystals of bacterial L-lactate dehydrogenase reveal the mechanism for allosteric control. Nat. Struct. Biol. 1, 176-185.

James, L. C., Tawfik, D.S. (2003). Conformational diversity and protein evolution-a 60-year-old hypothesis revisited. Trends Biochem. Sci. 28, 361-368.

Jiao, W., Blackmore, N. J., Nazmi, A. R., Parker, E. J. (2017). Quaternary structure is an essential component that contributes to the sophisticated allosteric regulation mechanism in a key enzyme from *Mycobacterium tuberculosis*. PLoS ONE 12(6), e0180052.

Kabsch, W. (2010). XDS. Acta Crystallogr. D. 66,125–132.

Kalimeri, M., Girard, E., Madern, D., Sterpone, F. (2014). Interface Matters, the Stiffness Route to Stability of a Thermophilic Tetrameric Malate Dehydrogenase. PLoS ONE 9(12), e113895.

Katava, M., Maccarini, M., Villain, G., Paciaroni, A., Sztucki, M., Ivanova, O., Madern, D., Sterpone, F. (2017). Thermal activation of 'allosteric-like' large-scale motions in a eukaryotic Lactate Dehydrogenase. Sci. Rep. 7, 41092.

Konarev, P. V. Volkov, V. V., Sokolova, A. V. Koch, M. H, J., Svergun, D. (2003). *PRIMUS*, a Windows PC-based system for small-angle scattering data analysis. J. Appl. Cryst. 36, 1277-1282.

Krissinel, E. (2015). Stock-based detection of protein oligomeric states in jsPISA. Nucleic Acids Res. 43, 314-319.

Kumawat, A., Chakrabarty, S. (2017). Hidden electrostatic basis of dynamic allostery in a PDZ domain. Proc. Natl. Acad. Sci. U S A 114, 5825-5834

Langelandsvik, A. S., Steen, I. H., Birkeland, N. K., Lien T. (1997) Properties and primary struture of a thermostable L-malate dehydrogenase from Archaeoglobus fulgidus. Arch. Microbiol. 168, 59-67.

Lee, D., Hong, J., Kim, K. J. (2019). Crystal structure and biochemical characterization of malate dehydrogenase from *Metallosphaera sedula*. Biochem Biophys. Res. Com. 509, 833-838.

Madern, D. (2000). The putative L-lactate dehydrogenase from Methanococcus jannaschii is a NADPH-dependent L-malate dehydrogenase. Mol Microbiol. 37, 1515-1520

Madern, D. (2002). Molecular Evolution within the L-Malate and L-Lactate Dehydrogenase Super-Family. J. Mol. Evol. 54, 825-840

Madern, D., Cai, X. M., Abrahamsen, M. S., Zhu, G. (2004). Evolution of Cryptosporidium parvum lactate dehydrogenase from malate dehydrogenase by a very recent event of gene duplication. Mol. Biol. Evol. 21, 489-497.

Madern, D., Ebel, C., Mevarech, M., Richard, S. B., Pfister, C., Zaccai, G. (2000). Insights into the molecular relationships between malate and lactate dehydrogenases. Structural and biochemical properties of monomeric and dimeric intermediates of a mutant of tetrameric L-[LDH-like] malate dehydrogenase from the halophilic archaeon *Haloarcula marismortui.* Biochemistry 39, 1001-1010.

Marchler-Bauer, A. Lu, S., Anderson, J. B., Chitsaz, F., Derbyshire, M. K. et al. (2011). "CDD, a Conserved Domain Database for the functional annotation of proteins." Nucleic Acids Res. 39, 225-229.

Marsh, J. A., Teichmann, S. A. (2014). Protein flexibility facilitates quaternary structure assembly and evolution. Plos ONE 12(5), e1001870.

McCoy, A. J., Grosse-Kunstleve, R. W., Adams, P. D., Winn, M. D., Storoni, L. C., Read, R. J. (2007). *Phaser* crystallographic software. J. Appl Cryst. 40, 658-674.

Monod, J., Wyman, J., Changeux, J. P. (1965). On the nature of allosteric transitions, a plausible model. J. Mol. Biol.12, 88-118.

Motlagh, H. N., Wrabl, J. O., Li, J., Hilser, V. J. (2014). The ensemble nature of allostery. Nature 508, 331-339.

Nussinov, R., Tsai, CJ. (2015). Allostery without a conformational change? Revisiting the paradigm. Curr. Opin. Struct. Biol. 30, 17-24.

Ohta, T., Yokota, K., Minowa, T., Iwata, S. (1992). Mechanism of allosteric transition of bacterial L-lactate dehydrogenase. Faraday Disc. 93, 153-162.

Painter, J., Merritt, E. A. (2005). A molecular viewer for the analysis of TLS rigid-body motion in macromolecules. Acta Cryst. D. 61, 465-471.

Painter, J., Merritt, E. A. (2006). Optimal description of a protein structure in terms of multiple groups undergoing TLS motion. Acta Cryst. D. 62, 439-450.

Rossmann, M. G., Adams, M. J., Buehner, M., Ford, G. C., Hackert, M. L., Liljas, A., Rao, S. T., Banaszak, L. J., Hill, E. Tsernoglou, D., Webb, L. (1973). Molecular symmetry axes and subunit interfaces in certain dehydrogenases. J. Mol. Biol. 77, 533-537.

Singh, A. K., Manjasetty, B., Koul, S., Kaushik, A., Ekka, M. K,, et al. (2015). Crystal Structure of Fad35R from *Mycobacterium tuberculosis* H37Rv in the Apo-State. PLoS ONE 10(5), e0124333.

Svergun, D., Barberato, C., Koch, M. H. J. (1995). *CRYSOL* - a Program to Evaluate X-ray Solution Scattering of Biological Macromolecules from Atomic Coordinates. J. Appl. Cryst. 28, 768-773.

Taguschi, H. (2017). The Simple and Unique Allosteric Machinery of Thermus caldophilus lactate dehydrogenase, structure-function relathionship in bacterial allosteric LDHs. Adv. Exp. Med. Biol. 925,117-145.

Theobald, D. L., Steindel, P. A. (2012). Optimal simultaneous superpositioning of multiple structures with missing data. Bioinformatics 28, 1972-1979.

Theobald, D. L., Wuttke, D. S. (2006). THESEUS, maximum likelyhood superpositioning and analysis of macromolecular structures. Bioinformatics 22, 2171-2172

Theobald, D. L., Wuttke, D. S. (2008). Accurate Structural Correlations from Maximum Likelihood Superpositions. PLoS Comp. Biol. 4(2): e43.

Tomita, T., Kuzuyama, T., Nishiyama, M. (2006). Alteration of coenzyme specificity of lactate dehydrogenase from Thermus thermophilus by introducing the loop region of NADP(H)-dependent Malate dehydrogenase. Biosci. Biotechnol Biochem 70, 2230-2235.

Waldman, A. D. B., Hart, K. W., Clarke, A. R., Wigley, D. B., Barstow, D. A., Atkinson, T., Chia, W.N., Holbrook, J. J. (1988). The use of a genetically engineered tryptophan to identify the movement of a domain of *Bacillus stearothermophilus* lactate dehydrogenase with the process which limits the steady-state turnover of the enzyme. Bio. Bioph. Res. Com. 150, 752-759.

Wilks, H. M., Hart, K. W., Feeney, R., Dunn, C. R., Muirhead, H., Chia, W. N., Barstow, D. A., Atkinson, T., Clarke, A. R., Holbrook, J. J. (1988). A specific, highly active malate dehydrogenase by redesign of a lactate dehydrogenase framework. Science 242, 1541–1544.

Wilson, D., Pethica, R., Zhou, Y., Talbot, C., Vogel, C., Madera, M., Chothia, C., Gough, J. (2009). SUPERFAMILY-sophisticated comparative genomics, data mining, visualization and phylogeny. Nucl. Ac. Res. 37, 380-386.

Winn, M. D., Ballard, C. C., Cowtan, K.D., Dodson, E. J., Emsley, P.,et al., (2011). Overview of the CCP4 suite and currents developments. Acta Cryst. D 67, 232-242.

SUPPLEMENTARY DATA

The archaeal LDH-like malate dehydrogenase from *Ignicoccus islandicus* displays dual substrate recognition, hidden allostery and a non-canonical tetrameric oligomeric organization.

Jennifer Roche[1], Eric Girard[1], Caroline Mas[1] and Dominique Madern[1]

[1] Univ. Grenoble Alpes, CEA, CNRS, IBS, 38000 Grenoble, France

* Corresponding author:

Dr Dominique Madern, Institut de Biologie Structurale, Campus EPN CS 10090, 71 avenue des Martyrs, 38044 Grenoble Cedex 9; France.

Email: dominique.madern @ ibs.fr. Phone: 33- (0) 4 57 42 85 71.

Fig. S1. Structure-based sequence alignment. The primary sequences of enzymes of i) LDH from *Bacillus stearothermophilus, Bifidobacterium longum* and *Thermus thermophilus* (*B. ste*, *B. lon* and *T. the* LDH, respectively); ii) MalDHs from *Ignicoccus islandicus*, *Methanosphera sedula, Chlorobaculum tepidum, Methylobacterim extorquens* and *Methanocaldococcus jannaschii* (*I. isl*, *M. sed*, *C. tep, M. ext and M. jan* MalDH, respectively) were aligned as described in materials and methods. Important residues in red and the amino acid region underlined (allosteric core) are discussed in the main body of the manuscript. The sequence

numbering refers to the LDH nomenclature. The secondary structure elements of *T. the* LDH are marked above the sequences: helices are identified by h and beta strands by s.

Fig. S2. Treatment of *I. isl* MalDH SAXS data using PRIMUS (ATSAS program suite). All data shown are coming from the chimera curve merged from a low (0.39 mg/ml) and a high (9.31 mg/ml) concentration of *I. isl* MalDH. (A) Chimera scattering curve. Error bars, computed from standard deviation data, are represented in pink. (B) Guinier plot. Standard deviations values from the fitted line are reported in green, on a horizontal line. The corresponding Y-axis is on the right side of the plot. (C) Dimensionless Kratky plot. (D) Distance distribution function of particle.

Fig. S3. Comparison between experimental SAXS data of *I. isl* MalDH with theoretical curves from various models using CRYSOL. SAXS experimental data are represented by red dots. (A) SAXS theoretical data calculated from the same atomic model of the *I. isl* MalDH as indicated in Figure 4 (green line). Theoretical curves calculated from atomic model of *I. isl* MalDH build on i) *T. the* LDH structure (2V6M) (pink line), ii) *C.tep* MalDH structure (1GUZ) (blue line) as template respectively. χ^2 values are written beside the corresponding models used. (B) *I. isl* MalDH theoretical curve as in panel a, and theoretical curve calculated from *M. sed* MalDH crystal structure (Accession PDB ID: 6IHD) (blue line).

Fig. S4.

Close-up view of electron density around the lateral chain of the substrate-binding residue (Arg171 accordingly to LDH nomenclature) in *I. isl* MalDH structure. The 2Fo-Fc electron density map, contoured at 1σ, is colored in blue. Small red spheres represent water molecules.

Table S1. Data collection and refinement statistics of the *I. isl* MalDH structure. Statistics for the highest-resolution shell are shown in parentheses.

Table S2. *I. isl* MalDH SAXS data.

Table S3. Interface analyses of *I. isl* MalDH, *C. tep* MalDH and *T. the* LDH structures using PISA qt-interfaces (CCP4 program suite). Values are given in A^2.

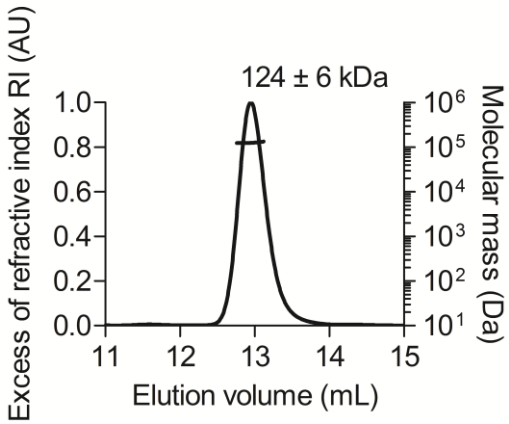
124 ± 6 kDa
Excess of refractive index RI (AU)
1.0
0.8
0.6
0.4
0.2
0.0
11
12
13
14
15
Elution volume (mL)
10^6
10^5
10^4
10^3
10^2
10^1
Molecular mass (Da)

Fig. 1.

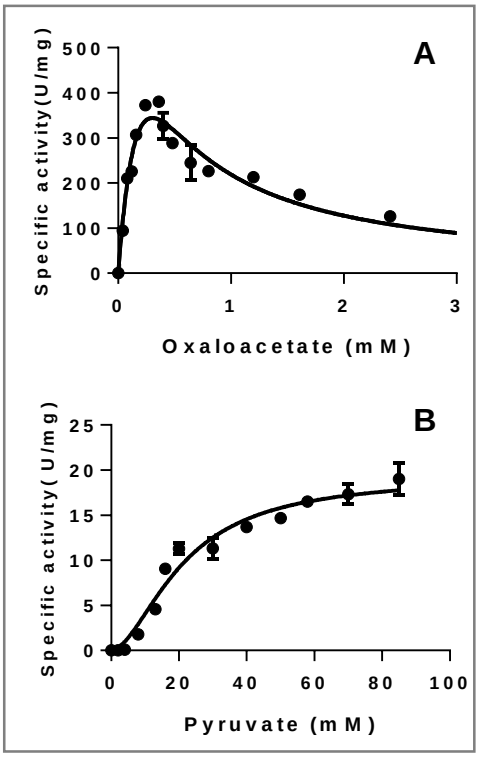
A
Specific activity(U/mg)
500
400
300
200
100
0
0
1
2
3
Oxaloacetate (mM)
B
Specific activity(U/mg)
25
20
15
10
5
0
0
20
40
60
80
100
Pyruvate (mM)

Fig. 2.

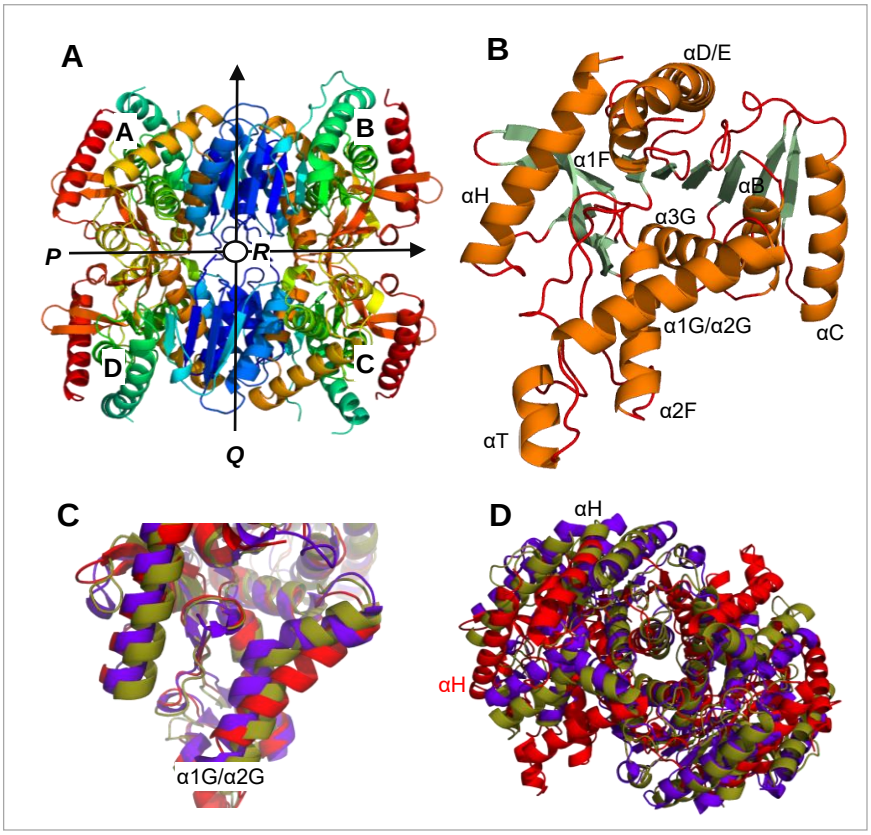

Fig. 3.

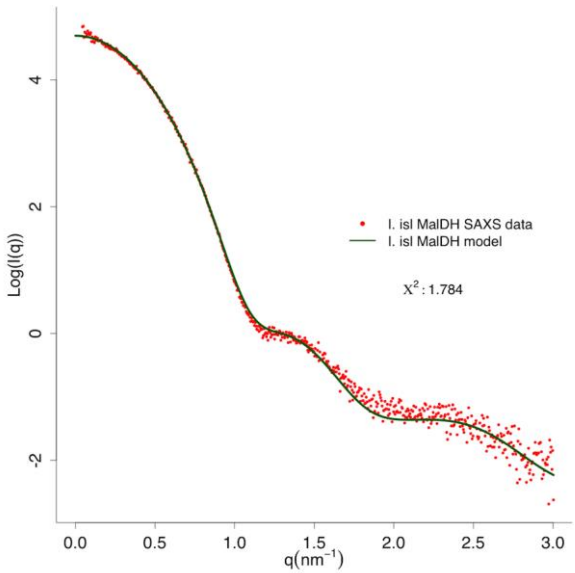
I. isl MalDH SAXS data
I. isl MalDH model
X²: 1.784
Log(I(q))
q(nm⁻¹)
4
2
0
-2
0.0
0.5
1.0
1.5
2.0
2.5
3.0

Fig. 4.

A

	Crenarchaeal MalDH		Canonical MalDH	Canonical LDH	
Structure	***M. Sed*** **binary form**	***M. Sed*** **ternary form**	***C. Tep***	***T. The*** **T-state**	***T. The*** **R-state**
RMSD (Å²)	1.51	1.57	15.20	14.22	12.14

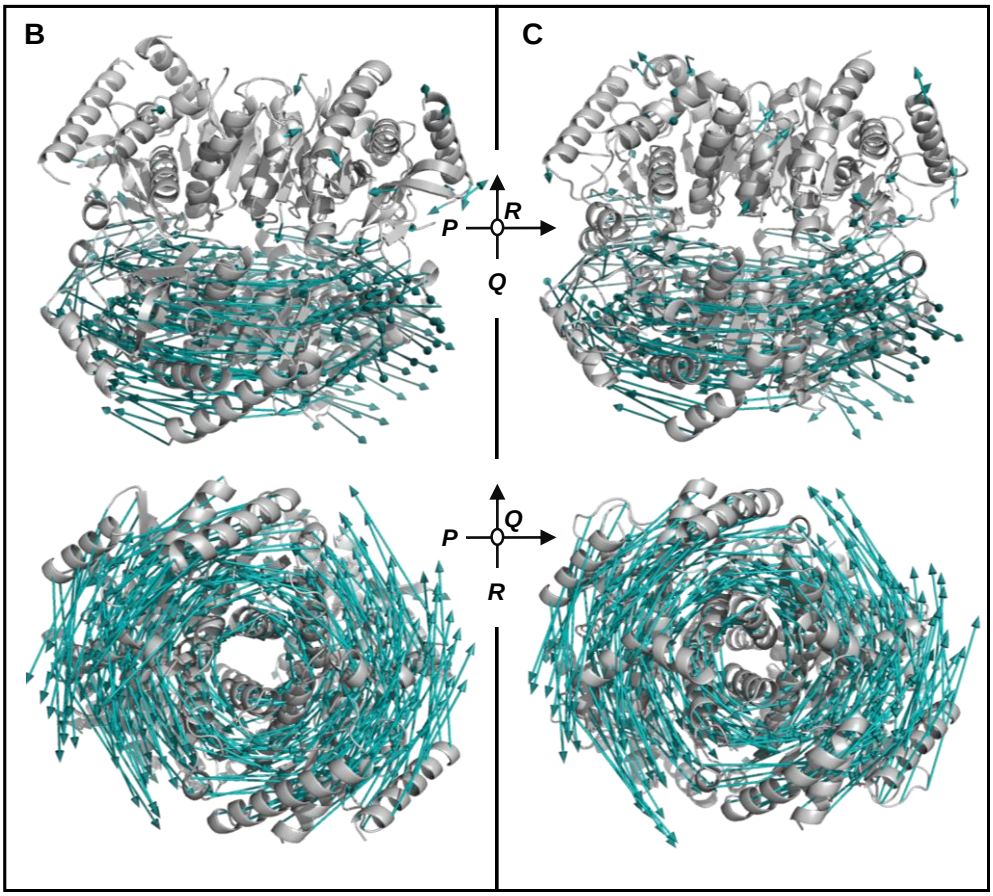

Fig. 5.

A

		68	102	168	171	195	199	246
LDH	**T. the**	H	Q	D	R	H	E	T
MalDH	**I. isl**	H	R	D	R	H	A	T
	M. sed	H	R	E	R	H	A	T
	C. tep	D	R	D	R	H	M	A

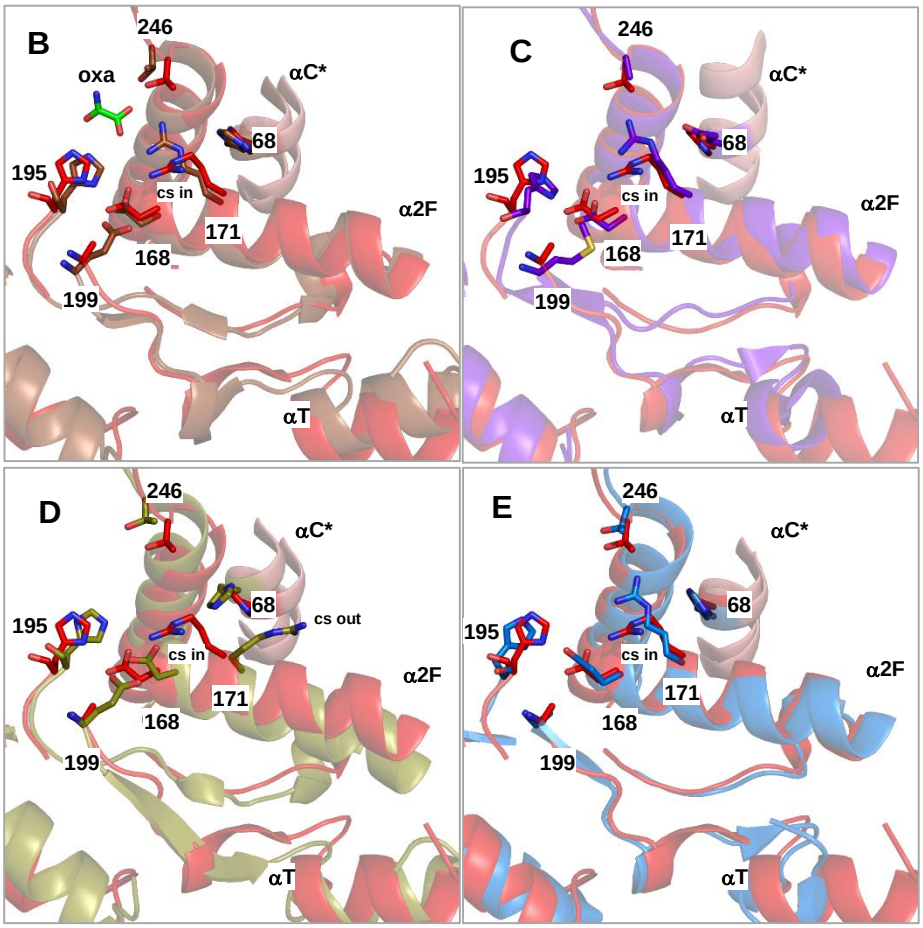

Fig. 6.

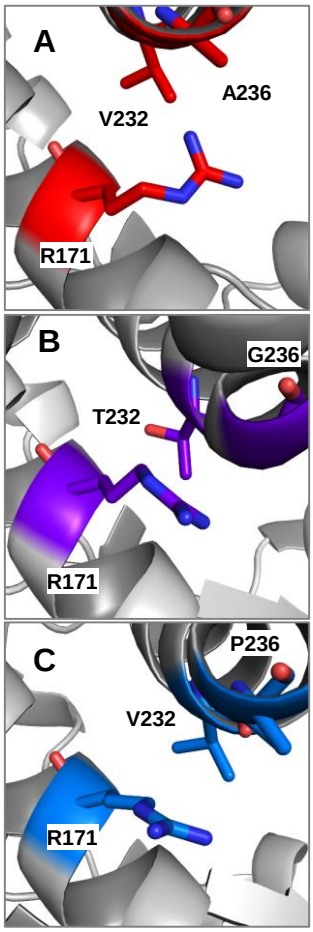

Fig. 7.

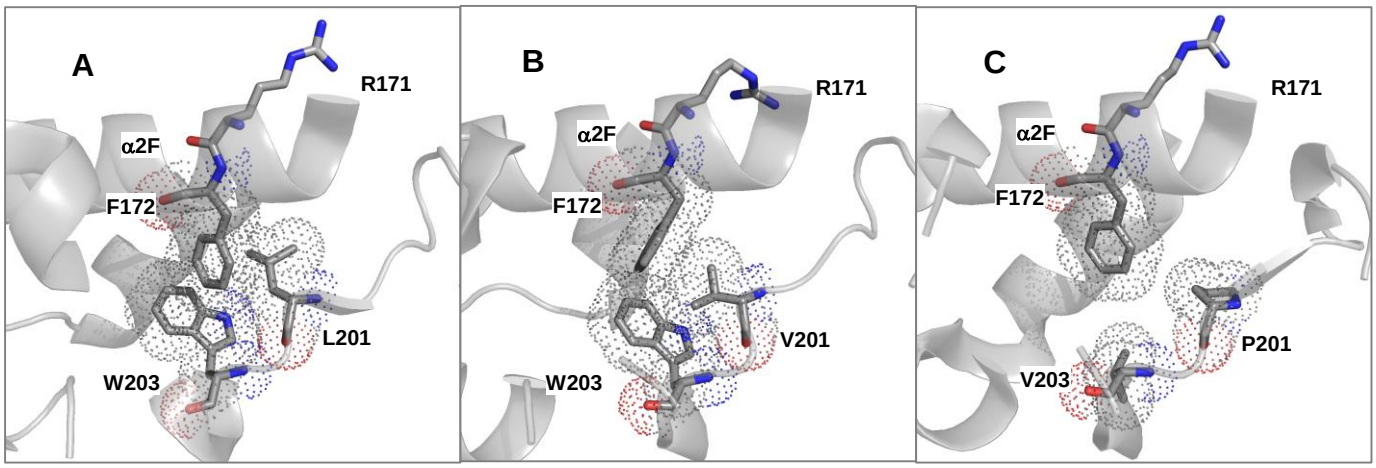
A
R171
α2F
F172
L201
W203
B
R171
α2F
F172
V201
W203
C
R171
α2F
F172
P201
V203

Fig. 8.

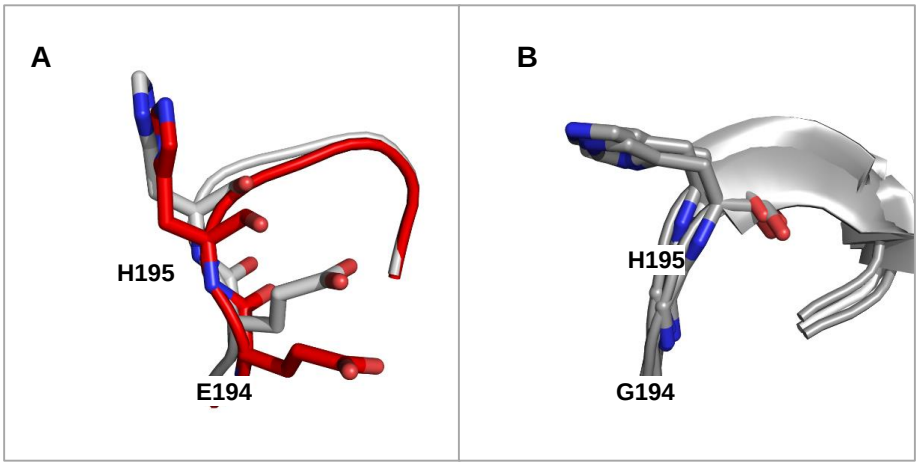

Fig. 9.

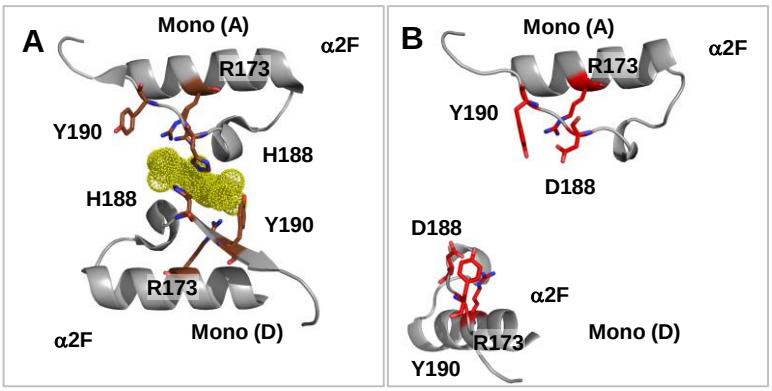
A
Mono (A)
α2F
R173
Y190
H188
H188
Y190
R173
α2F
Mono (D)
B
Mono (A)
α2F
R173
Y190
D188
D188
α2F
R173
Mono (D)
Y190

Fig. 10.

	Oxaloacetate	Pyruvate
k_{cat} (s^{-1})	444	8
K_m (m*M*)	0.38	
K_i (m*M*)	0.24	
$S_{0.5}$ (m*M*)		21
k_{cat}/K_m (M^{-1} s^{-1})	1.2×10^6	
$k_{cat}/S_{0.5}$ (M^{-1} s^{-1})		0.37×10^3

Table 1.